

Sim-source for 4D: Learnings from processing the first ISS OBN monitor survey at Atlantis

Jing Yang*, Xin He, Jiawei Mei, Rongxin Huang (CGG); Qingsong Li, Kang Fu, Jean-Paul van Gestel (bp)

Summary

Driven by the notion that blending noise may materially increase the background noise level and obscure the interpretation of weak time-lapse (4D) signals related to subtle reservoir changes, the industry has not yet seen any simultaneous-source (sim-source) surveys acquired for reservoir monitoring. Thus, whether sim-source acquisition is feasible for 4D remains a long-standing question. In 2019, bp took the step forward by acquiring the first sim-source ocean bottom node (OBN) monitor survey at the Atlantis field in the Gulf of Mexico (GoM). With 4D-friendly deblending and matching of sources from different vessels, we were able to mitigate the challenges associated with the 2019 independent simultaneous source (ISS) OBN survey and obtain a similar level of 4D signal-to-noise ratio (S/N) and valuable 4D signals comparable to what we could achieve with conventional OBN data. Further, meaningful subsalt 4D signals were revealed for the first time in the areas with fairly poor illumination even with the 2019 ISS OBN survey, partly due to the larger reservoir changes from a longer production history and a more accurate velocity built from full-waveform inversion (FWI).

Introduction

OBN acquisition has been regarded as the preferred solution for reservoir monitoring due to its excellent repeatability of shot and receiver positions. However, the application of OBN is still often limited by its high cost, as it acquires dense shot carpets and uses a remotely operated vehicle (ROV) for node deployment. Sim-source technology has been proposed to improve the acquisition efficiency and, thus, reduce the acquisition cost. Many previous studies have demonstrated the effectiveness of deblending to attenuate the blending noise in sim-source OBN data and have established that sim-source OBN data after deblending can produce 3D images of similar quality as those from conventional acquisition (Abma et al., 2012; Alexander et al., 2013; Zhuang et al., 2017). Therefore, sim-source has become the norm for OBN surveys in recent years due to its proven success in 3D imaging and reduced acquisition cost. However, whether a sim-source survey is good enough for 4D monitoring remains a question in the industry. As an increasing number of sim-source OBN surveys are acquired, and given that many of them will likely become baseline or monitor surveys for future 4D programs, the industry urgently needs an answer to this question. Although the feasibility of sim-source OBN 4D has been demonstrated on a synthetic study (Davies and Ibram, 2015), a sim-source OBN survey for 4D had not previously been acquired, likely hindered by the possibility that the blending noise may materially increase the background noise level and obscure the interpretation of weak 4D signals.

In 2019, bp took the step forward by acquiring the first ISS OBN monitor survey at Atlantis in the deepwater GoM, in which two source boats with two sources on each boat fired

independently. In addition to using this sim-source survey, our 4D study included two other OBN surveys, a baseline and a monitor, that were acquired over the Atlantis field in 2005 and 2015, respectively (Table 1). There is also another OBN data set acquired in 2009, but it was not included in this study. These two conventional OBN surveys have provided high-quality 4D data in the well-imaged extra salt area, which shows clear hardening and softening signals related to water movement and pressure changes in different levels of reservoirs (Van Gestel and Anderson, 2017). The latest 2019 survey acquired a total of 2948 nodes within 31 days, which included 1247 repeated nodes of the 2015 survey, 1224 dense nodes to improve S/N of the 3D image, and 485 nodes at the outer ring to record long-offset data from the Wolfspaar source for FWI velocity update (Dellinger et al., 2016; Ni et al., 2019) (Table 1). The objective of the 2019 monitor survey was to continue to monitor reservoir changes related to production and water injection since the last monitor survey and to validate the feasibility of sim-source for 4D. In the following sections, we will share the results and learnings from processing this sim-source 4D survey.

	Baseline (2005)	Monitor 1 (2015)	Monitor 2 (2019) ISS
Number of Nodes	1628 nodes	1908 nodes	Total 2948 nodes (1247 repeated nodes)
Acquisition Patches	2	1	1
Number of Source boats	1	1	2
Source Size	4330 inch ²	4330 inch ²	5110 inch ²
Source Array Depth	15m	15m	15m
Shot spacing	53.7m	53.7m	53.7m
Source Area	~760 km ²	~1200 km ²	~678 km ²
Node Area	247 km ²	289 km ²	189 km ² for 4D nodes
Node spacing	426mx369m	426mx369m	213mx369m
Acquisition duration	122 days	95 days	31 days

Table 1: Acquisition parameters

4D-friendly Deblending

Deblending is inevitably the most critical step for the success of sim-source 4D. The 2019 Atlantis OBN survey was acquired using two types of sources – a low-frequency vibratory Wolfspaar source from a separate boat and four conventional airgun sources from the other two source boats. In order to deblend data of multiple source types, we generalized our deblending algorithm by constructing signals for each seismic source type separately during the inversion (Fu et al., 2019). Since the Wolfspaar source only emits low-frequency signals, Wolfspaar deblending was only performed in the low-frequency band (< 3.5 Hz) jointly with airgun deblending in the same frequency range to separate the Wolfspaar data from the airgun data. After Wolfspaar deblending, we subtracted the Wolfspaar energy from the airgun data and moved on to airgun deblending in the full frequency band. All of the above deblending steps employed a hybrid deblending algorithm (Zhuang et al., 2017), which includes 3D FK domain iterative signal picking and impulsive denoising with the guidance of a noise-signal-

Sim-source for 4D

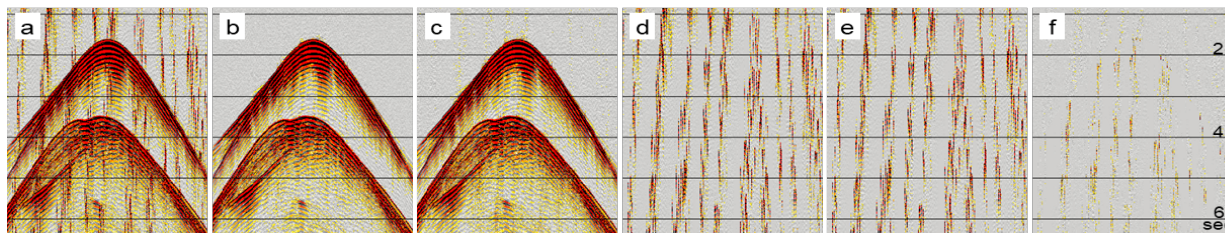


Figure 1: Common receiver gathers of the P component (a) before deblending, (b) after conventional deblending, (c) after 4D-friendly deblending, (d) noise attenuated from conventional deblending, (e) noise attenuated from 4D-friendly deblending, (f) difference between (b) and (c).

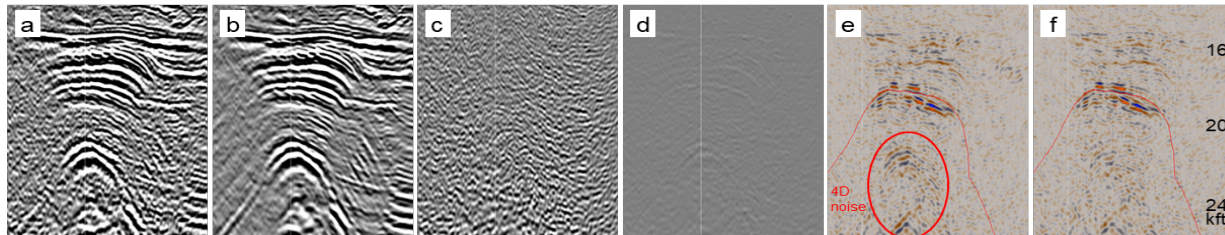


Figure 2: Section view of 2019 OBN 25 Hz RTM (a) before deblending, (b) after conventional deblending or 4D-friendly deblending (c) difference from conventional deblending or 4D-friendly deblending (3D image and deblending difference from both deblending are nearly identical) (d) difference between conventional deblending and 4D-friendly deblending, and the 2019-2005 4D difference (e) after conventional deblending, (f) after 4D-friendly deblending. 4D difference volumes were generated after fast-track 4D processing flow including demultiple. Red line indicates the main reservoir.

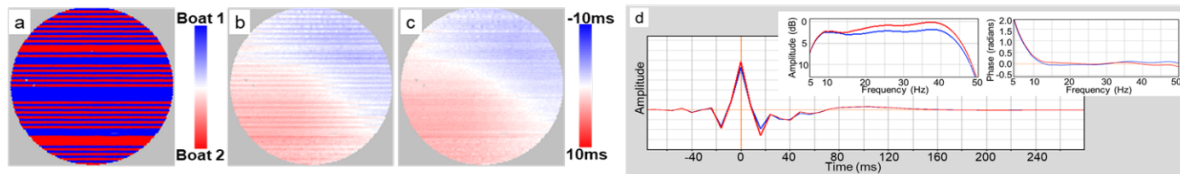


Figure 3: Map for the shots within a 3 km offset range of one node (a) boat ID map: red and blue represented two different source vessels, (b) dT map, (c) dT map after 1 ms time shift applied on one of the source vessels. (d) The stacked wavelets from two different source vessels.

ratio (NSR) map. Figures 1b, 1d and Figures 2b, 2c show blending noise was reasonably removed without noticeable signal damage in both data and image domains after Wolfspär deblending and conventional airgun deblending. However, potential signal damage could be buried under the strong background blending noise, which makes it difficult to observe any signal damage in pre-migration data and even in 3D migration images. In order to QC the results of conventional deblending, we further performed a fast-track 4D processing flow including demultiple and generated the 2019-2005 4D difference (Figure 2e). There is coherent 4D noise evident, as highlighted by the red circle in Figure 2e. This coherent 4D noise indicates that potential signal damage happened in the conventional airgun deblending process, since any signal damage in the time domain will appear as coherent 4D noise in the image domain. Unlike random noise or migration swings that can be effectively attenuated by post-migration co-denoise (Huang et al., 2014), this type of coherent 4D noise is challenging to attenuate and can obscure 4D interpretation. Hence, better preservations of signals in the deblending process will be needed for subsequent 4D processing.

In order to better preserve primaries, we improved our airgun deblending process by using stricter signal picking parameters with more iterations for better signal modeling

and optimized thresholds for the NSR map in impulsive denoise. Although the new deblending left slightly more residual blending noise in the data domain (Figure 1c), the migration image and deblending difference from the new deblending are nearly identical to those from conventional deblending. More importantly, the new deblending, which better preserved primaries, significantly reduced the background coherent 4D noise in the 2019-2005 4D difference (Figure 2f) and resulted in a $\sim 2\%$ NRMS drop at the target area. Deblending with improved primary preservation, followed by 4D QC, is the key to obtaining a 4D-friendly deblending result for sim-source 4D.

Source inconsistency between different vessels

Even though the airgun arrays for the two source boats were configured identically, some inconsistencies between the sources from different vessels were observed. These can cause issues in the 4D repeatability and need to be addressed. First, the timing difference between sources from different vessels was clearly illustrated by the dT map of the 2019 data (Figures 3a-c). dT is the misfit between calculated direct arrival time and measured direct arrival time, and is the key input for the inversion and correction of water velocity, node/shot position, and node clockdrift (Amini et al., 2016; Huang et al., 2016), which are crucial steps in deepwater 4D projects for increasing 4D repeatability. The stripe pattern

Sim-source for 4D

on the dT map caused by the timing difference between sources from different vessels could potentially introduce errors in traveltimes inversion. Further, the stacked down-going water bottom wavelets revealed amplitude and phase spectra differences between sources from different vessels (Figure 3d). This source inconsistency from different vessels must be addressed prior to traveltimes inversion and matching between 4D surveys. One matching filter derived from stacked wavelets and one constant time shift were used to alleviate the source inconsistency of the 2019 ISS data. The matching of sources from different vessels helped to mitigate potential errors in traveltimes inversion, increase the integrity of the 2019 ISS data, and improve the 4D repeatability of the sim-source survey.

Results

All three OBN surveys were consistently processed from raw data except that deblending and matching of sources between different vessels were applied on the 2019 data only. The latest velocity model from Time-Lag FWI (TLFWI), which resolved the complex salt geometry and led to significant uplifts in the 3D image (Zhang et al., 2018; Mei et al., 2019), was used for down-going wavefield Reverse Time Migration (RTM). Since only the 2019 survey is a sim-source survey, the 2015-2005 4D will hereafter be referred to as a conventional 4D case and the 2019-2005 4D and 2019-2015 4D will be referred to as sim-source 4D cases. NRMS maps of raw RTM without any post-migration processing for these three 4D cases are compared in Figure 4. Median values of background NRMS at the water bottom and reservoir are in a very similar range (~6%) with variation less than 0.5%. Note that due to the presence of 4D signals, NRMS outside of the reservoir was used for background noise evaluation. There is no clear indication that the conventional 4D case has lower background noise than the sim-source 4D cases. The final 4D difference volumes in section view are compared in Figure 5. There is also a similar level of background 4D noise for these three 4D cases. Since more wells were in production at the shallow reservoir after 2015, new 4D responses, marked by the black arrows above the mid reservoir (indicated by the red horizon) in Figure 5, appear as expected in the 4D difference from the 2019 ISS data.

At the Atlantis field, strong hardening response is usually due to the increase of water saturation, while softening response is an indication of large pressure depletion (Van Gestel et al., 2017). Amplitude extractions from the 4D difference volumes were used for the interpretation of water movement and pressure change at the reservoirs. As expected, hardening responses above the original oil-water contact (OOWC) are clearly visible on both the 2015-2005 conventional 4D case and the 2019-2005 sim-source 4D case at the well-imaged extra salt area (Figure 6). Compared to the 2015-2005 4D case, the 2019-2005 4D case showed more hardening response updip of the OOWC in all three reservoirs and more softening responses at the shallow reservoir. The northern parts of the reservoirs are located directly below complex salt fingers, and both 3D images and

4D differences have previously been quite poor at the subsalt area due to velocity errors, poor illumination, and low S/N. With a more accurate velocity model from TLFWI and after a longer production history, subsalt 4D signals are observed for the first time in the 2019-2005 sim-source 4D case. Hardening signals due to water movement are clearly visible at the subsalt area (marked by black arrows in Figures 6e and 6h). The observations obtained with the 2019 ISS OBN survey provide meaningful information of reservoir changes and are helpful for future well planning at the Atlantis field.

Conclusions and discussions

We demonstrated that the 2019 ISS OBN survey was able to provide a similar level of 4D S/N and valuable 4D signals comparable to a conventional OBN survey after the blending noise and source inconsistencies from the sim-source survey were addressed. Meaningful 4D signals were obtained not only at the well-imaged extra salt area but also at the poorly illuminated subsalt area in the sim-source 4D case. However, blending noise and source inconsistency are only two of the non-repeatable factors in sim-source 4D surveys. Remaining errors from other non-repeatable factors as we would have in conventional 4D surveys, such as water velocity changes, source directivity, and shot-by-shot source variations, are highly survey dependent due to the limitations of algorithms and/or available data. These remaining errors could manifest differently in different 4D surveys and in different geologic settings, and may become more dominant sources of 4D noise and prevent us from seeing the full impact of sim-source for 4D.

Despite the drawbacks related to blending noise and source inconsistency, sim-source acquisition can provide some benefits for 4D. For instance, ambient background noise, which is shared between overlapping shots, may be reduced in the deblended data as opposed to conventional data. Moreover, due to the shorter acquisition time, the water velocity is likely to have less variation in sim-source surveys. More consistent water velocities during acquisition not only reduces the non-repeatable errors from the water column but also benefits some preprocessing steps, such as demultiple.

Although subsalt 4D signals can be observed with the 2019 ISS OBN survey, they still appear weaker, and the 4D noise level is still much higher than at the extra salt area due to poor illumination and lower S/N in the input data. As shown in the latest study (Zhang et al., 2020; Huang et al., 2021), FWI Imaging can provide an image of higher S/N and better-balanced illumination through the use of full-wavefield data and iterative least-squares data fitting. Thus, it is a good candidate for further improving 4D results, especially subsalt 4D results at Atlantis. Moreover, FWI Imaging can also be particularly beneficial for sim-source 4D surveys, as FWI results in general are not sensitive to blending noise.

Acknowledgments

We thank bp, BHP, and CGG for permission to publish this work.

Sim-source for 4D

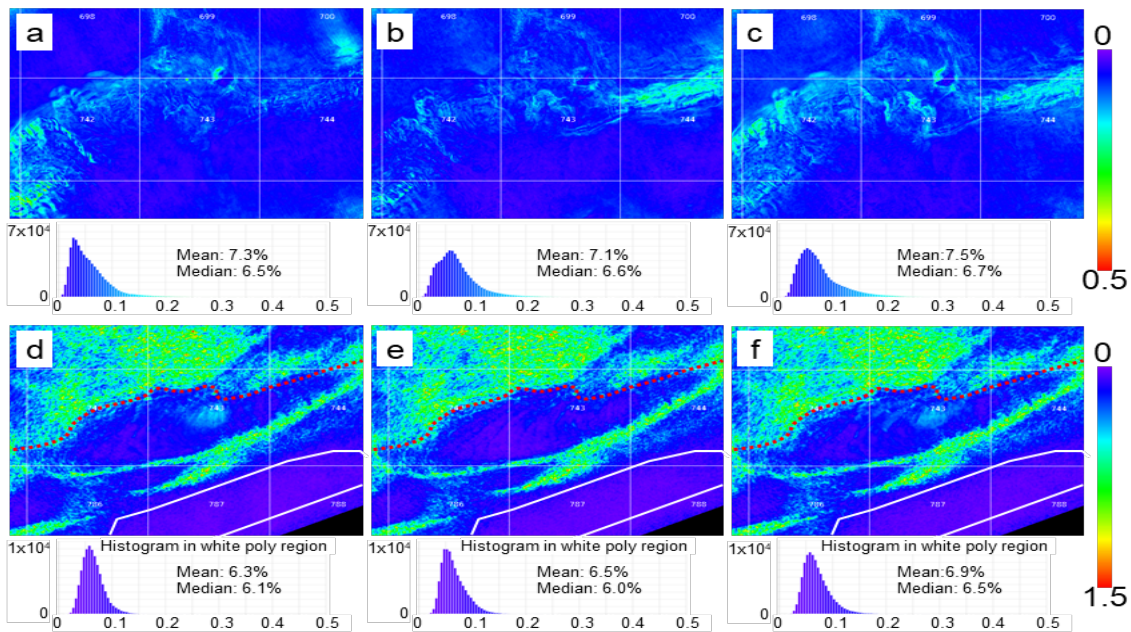


Figure 4: (a-c) NRMS maps around water bottom and their corresponding histograms and (d-f) NRMS maps around reservoir and their histograms for the area within the white polygon for various 4D pairs: (a,d) 2015-2005 4D, (b,e) 2019-2015 4D, (c,f) 2019-2005 4D. White polygon shows the region outside the reservoir. Red dotted line represents the southern edge of the salt.

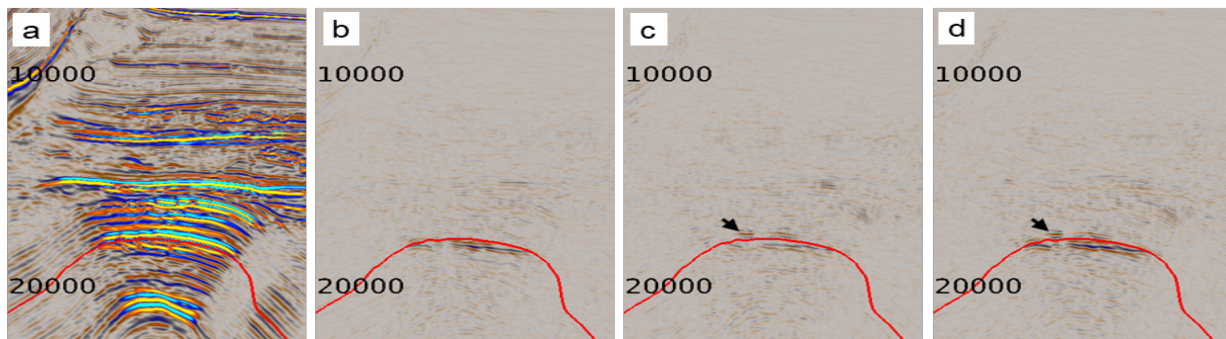


Figure 5: Section views of (a) 2005 final 25 Hz RTM 3D image, (b) 2015-2005 4D difference, (c) 2019-2015 4D difference, (d) 2019-2005 4D difference.

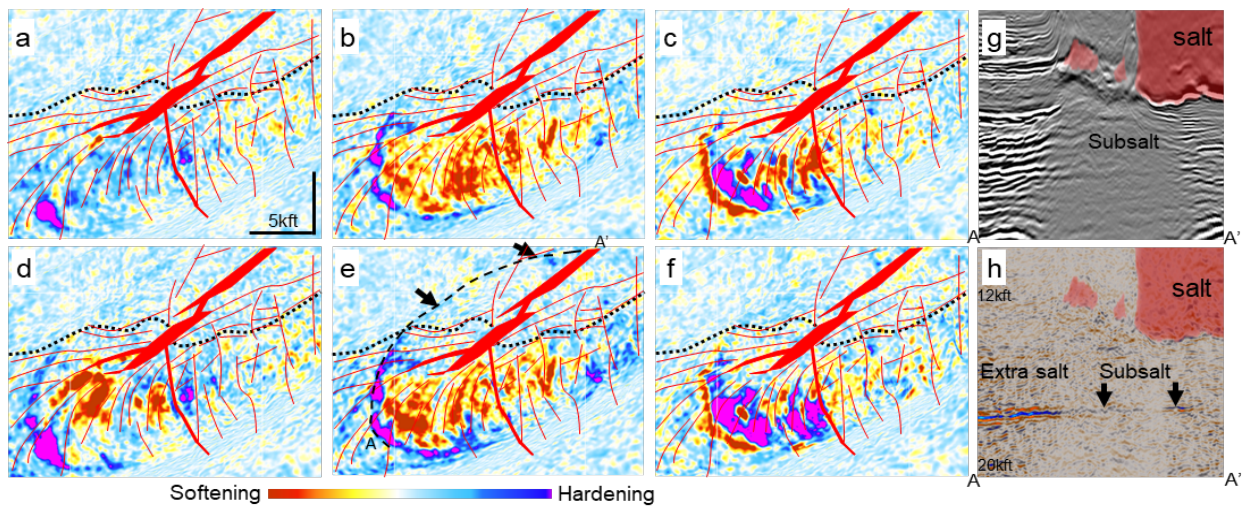


Figure 6: Amplitude extraction of 4D difference: (a,b,c) shallow, middle, and deep reservoirs for the 2015-2005 4D case; (d,e,f) shallow, middle, and deep reservoirs for the 2019-2005 4D case. (g,h) Fence section view along OOWC (Line A-A') of 2019 25 Hz RTM 3D image and the 2019-2005 4D difference. Red line and black dotted line represent fault polygon and the southern edge of the salt, respectively. Black arrows in e and h mark the potential subsalt 4D signals.

REFERENCES

- Abma, R., Q. Zhang, A. Arogunmati, and G. Beaudoin, 2012, An overview of BP's Marine Independent Simultaneous Source field trials: 82nd Annual International Meeting, SEG, Expanded Abstracts, 1–5, doi: <https://doi.org/10.1190/segam2012-1404.1>.
- Alexander, G., R. Abma, R. Clarke, S. W. La Dart, M. Corzo, K. Gulette, J. Mika, and J. Kommedal, 2013, Processing results of simultaneous source surveys compared to conventional surveys: 83rd Annual International Meeting, SEG, Expanded Abstracts, 104–108, doi: <https://doi.org/10.1190/segam2013-0641.1>.
- Amini, A., H. Peng, Z. Zhang, R. Huang, and J. Yang, 2016, Joint inversion of water velocity and node position for ocean bottom node data: 86th Annual International Meeting, SEG, Expanded Abstracts, 5490–5494, doi: <https://doi.org/10.1190/segam2016-13964730.1>.
- Davies, D. M., and M. Ibram, 2015, Evaluating the impact of ISS HD-OBC acquisition on 4D data: 77th Conference and Exhibition, EAGE, Extended Abstracts, We N101 05, doi: <https://doi.org/10.3997/2214-4609.201412870>.
- Dellinger, J., A. Ross, D. Meaux, A. Brenders, G. Gesoff, J. Etgen, J. Naranjo, G. Openshaw, and M. Harper, 2016, Wolfspar®, an “FWI-friendly” ultralow-frequency marine seismic source: 86th Annual International Meeting, SEG, Expanded Abstracts, 4891–4895, doi: <https://doi.org/10.1190/segam2016-13762702.1>.
- Fu, K., J. Dellinger, and R. Abma, 2019, Joint deblending of multiple seismic source types: 89th Annual International Meeting, SEG, Expanded Abstracts, 82–86, doi: <https://doi.org/10.1190/segam2019-3214753.1>.
- Huang, R., Y. Xuan, and C. Peng, 2014, Cooperative attenuation of non-repeatable noise in time-lapse processing: 84th Annual International Meeting, SEG, Expanded Abstracts, 4853–4857, doi: <https://doi.org/10.1190/segam2014-0563.1>.
- Huang, R., P. Wang, K. Nimsaila and M. Vu, 2016, Angle-dependent water column statics correction through sparse TauP inversion: 78th Conference and Exhibition, EAGE, Extended Abstracts, Tu LHR2 10, doi: <https://doi.org/10.3997/2214-4609.201600581>.
- Huang, R., Z. Zhang, Z. Wu, Z. Wei, J. Mei, and P. Wang, 2021, Full-waveform inversion for full-wavefield imaging: Decades in the making: The Leading Edge, **40**, 324–334, doi: <https://doi.org/10.1190/tle40050324.1>.
- Mei, J., Z. Zhang, F. Lin, R. Huang, P. Wang, and C. Mifflin, 2019, Sparse nodes for velocity: Learnings from Atlantis OBN full-waveform inversion test: 89th Annual International Meeting, SEG, Expanded Abstracts, 167–171, doi: <https://doi.org/10.1190/segam2019-3215208.1>.
- Ni, D., A. Brenders, J. Dellinger, J. Van Gestel, and Q. Li, 2019, Seismic modeling for a velocity survey at Atlantis: 89th Annual International Meeting, SEG, Expanded Abstracts, 182–186, doi: <https://doi.org/10.1190/segam2019-3215801.1>.
- Van Gestel, J., and G. Anderson, 2017, Integration of time lapse seismic observations into the reservoir model: A case study on Atlantis: 87th Annual International Meeting, SEG, Expanded Abstracts, 5850–5854, doi: <https://doi.org/10.1190/segam2017-17750100.1>.
- Zhang, Z., J. Mei, F. Lin, R. Huang, and P. Wang, 2018, Correcting for salt misinterpretation with full-waveform inversion: 88th Annual International Meeting, SEG, Expanded Abstracts, 1143–1147, doi: <https://doi.org/10.1190/segam2018-2997711.1>.
- Zhang, Z., Z. Wu, Z. Wei, J. Mei, R. Huang and P. Wang, 2020, FWI Imaging: Full-wavefield imaging through full-waveform inversion: 90th Annual International Meeting, SEG, Expanded Abstracts, 656–660, doi: <https://doi.org/10.1190/segam2020-3427858.1>.
- Zhuang, D., G. Shao, A. Khalil, B. Nolte, P. Paramo, and K. Vincent, 2017, Deblending OBC data with dual and triple simultaneous sources offshore Trinidad: 87th Annual International Meeting, SEG, Expanded Abstracts, 4914–4918, doi: <https://doi.org/10.1190/segam2017-17739616.1>.